doi:10.3772/j.issn.1006-6748.2017.02.003

A novel symmetrical 3-DOF PKM and its performance comparison with 3-PRS PKM①

Liu Yuzhe (刘宇哲)[*,**], Wu Jun②[*,**], Wang Liping[*,**], Zhao Jingshan[*], Wang Jinsong[*,**], Yu Guang[*,**]
([*] State Key Laboratory of Tribology and Institute of Manufacturing Engineering, Department of Mechanical Engineering, Tsinghua University, Beijing 100084, P. R. China)
([**] Beijing Key Laboratory of Precision/Ultra-precision Manufacturing Equipments and Control, Beijing 100084, P. R. China)

Abstract

A novel symmetrical 3-degree-of-freedom (DOF) parallel kinematic manipulator (PKM) is firstly presented, which is named 3-P (Qu) RU. According to the structure feature, a double closed loop vector method is proposed to investigate this PKM. Based on this method, kinematic, velocity and error models of this manipulator are established respectively. Since3-PRS PKM has been applied successfully in practice and its structure is similar to the 3-P (Qu) RU PKM, corresponding models of a 3-PRS PKM are given and a performance comparison study between them is investigated on workspace, manipulator dexterity, position error and error sensitivity. The comparison results reveal that the 3-P (Qu) RU PKM has the advantage on velocity performance and the disadvantage on accuracy performance. This novel 3-P (Qu) RU PKM is an available selection for a tool head of a hybrid machine tool and the analysis is greatly helpful for the further applications of this manipulator.

Key words: comparison study, parallel kinematic manipulator(PKM), kinematics, velocity, error

0 Introduction

It is well known that the parallel kinematic manipulator (PKM) has potential advantages in high speed, heavy load handling and high response rate. Its drawback is on the limited workspace. On the contrary, the serial kinematic manipulator (SKM) has the advantage of large workspace and the disadvantage of what PKM owns[1,2]. With an increasing need for manufacturing structural aircraft parts, hybrid machine tools, combining the advantages of PKMs and SKMs, are becoming a research hotspot and attracting more and more attentions from both academia and industry. The successful applications include ECOSPEED series machine centers developed by DS-Technologie[3], the Tricept series machine developed by PkmtriceptSL[4] and the TriVarianthybrid PKM proposed by Huang[5]. Usually as tool heads of hybrid machine tools, PKMs with different structures are investigated widely. Among a mass of PKMs, the 3-degree-of-freedom (DOF) PKMs are used most frequently and are most suitable due to their simple kinematics[6].

The structure of 3-DOF PKMs can be mainly divided into asymmetrical and symmetrical structures. Asymmetrical structures have been proposed and analyzed by a lot of researchers. A hybrid machine tool with a 3-DOF parallel module, TripteorX7, was proposed and its static and dynamic models were set up[7]. The proposed models predicted the behavior of the structure and avoided costly trials. A 2-UPS-PRP PKM was investigated and its error analysis revealed that some identified workspace either amplified or reduced the input errors[8]. In addition, future work about accuracy evaluation, static forces and kinematics were mentioned. A novel asymmetrical 3-DOF PKM with two translational and one rotational motions was designed[9]. This structure, which could rotate 360 degrees around the *Y*-axis, owned a higher rotational ability than general PKMs. A 2-PRU-PRRU PKM was created and studied on the aspect of kinematics[10]. Asymmetrical 3-DOF PKMs with 2-PRU-1PRS and 2-PRU-1PUR were respectively proposed by Xie[11]. Both of them aimed at a better orientation and elimina-

① Supported by the National Natural Science Foundation of China (No. 51575307, 51225503), the Science and Technology Major Project-Advanced NC Machine Tools & Basic Manufacturing Equipments (No. 2013ZX04004021, 2014ZX04002051) and Top-Notch Young Talents Program of China.

② To whom correspondence should be addressed. E-mail: jhwu@mail.tsinghua.edu.cn

Received on Apr. 5, 2016

ting parasitic motions. Another novel asymmetrical 3-DOF PKM, named TAM, with purely translational motions was presented and compared with the SKM400PKM on the conditional number of the Jacobin matrix[12]. An asymmetrical 3-DOF spherical PKM was studied in a mobility analysis[13]. The work provided plenty of theoretical foundations for different asymmetrical structures. Here, R, P, U and S represent revolute, prismatic, universal and spherical joint respectively.

However, asymmetrical 3-DOF structures may lead to an isotropic motions that are not suitable as a tool head in practice. In the successful applications in industry, symmetrical 3-DOF structures are more suitably used as a tool head like the Z3 tool head with a symmetrical 3-PRS structure in ECOSPEED and the symmetrical 3-UPS structure in Tricept. However, it is found that Tricept with an A/C-axis (rotations about the X- and Z-axes) tool head may scratch the finished surface during rotating the cutter in a high speed. Z3 with an A/B-axis (rotations about the X- and Y-axes) tool head avoids this problem. One can see that the symmetrical 3-PRS structure owns more advantages in the machining of aircraft structural parts. As far as the authors can be aware, vast literatures about kinematics and dynamics analysis[14], architecture optimization[15], dimension synthesis[16], and sensitivity analysis[17] were presented for the 3-PRS structure. However, few structure innovations based on the 3-PRS structure are presented. Although there are some structure innovations proposed such as in Ref. [18], these structures do not have a better kinematic performance than the 3-PRS structure and the structure innovations just rely on combinations of existing limbs or joints, which limits the further improvement on the comprehensive performances. In this paper, a novel 3-DOF symmetrical PKM, named 3-P (Qu) RU, derived from a 3-PRS structure is put forward. Qu joint is a kind of novel joint which is a planar quadrilateral construction with four revolute joints. This 3-P (Qu) RU PKM is analyzed in the aspects of workspace, velocity, position error and error sensitivity. So does the 3-PRS PKM. In order to show the performance of the 3-P (Qu) RUPKM clearly, a comparison study between the two PKMs is presented.

The remainder of the paper is organized as follows. The next section presents the descriptions and system modeling of a 3-P (Qu) RU PKM. The double closed loop vectors method is proposed to establish the system model. In Section 2, the 3-PRS PKM is introduced. In Section 3, in order to guarantee a fair comparison, a comparison rule is set up. Moreover, the evaluation indices are presented. In Section 4, numerical examples are utilized to show the comparison study. The conclusions are organized in Section 5.

1 Description and system modeling of 3-P (Qu) RU PKM

1.1 Description of configuration and calculation of DOF

A virtual prototype of the 3-P (Qu) RU PKM is shown in Fig. 1. It is composed of a mobile platform, a base platform, and three supporting limbs with an identical kinematic structure. Each supporting limb is composed of one P joint, one Qu joint, one R joint and one U joint. Qu joint is a novel joint, the target of which is to increase the stiffness of the manipulator. This joint is composed of four R joints and is a planar scissor like quadrilateral construction. The four R joints are installed at four vertices of the quadrilateral construction.

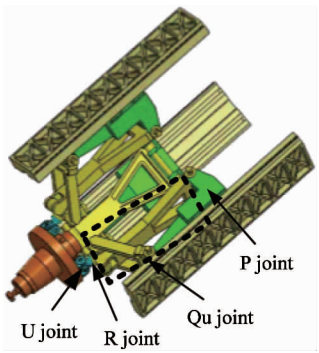

Fig. 1 The virtual prototype of 3-P (Qu) RU PKM

In order to determine the output motion of this PKM, its DOF number should be obtained. The formula for calculating the DOF of a manipulator is expressed as

$$NDOF = 6(n - g - 1) + f \quad (1)$$

where $NDOF$ represents the number of DOF in the manipulator, n represents the number of links, g represents the number of joints and f represents the total number of joint DOF.

As each limb is the same, Eq. (1) can be rewritten as

$$NDOF = 6(3n' + 2 - 3g' - 1) + 3k \quad (2)$$

where n' and g' represent the corresponding link and joint number of each limb, number 2 represents the link number for the mobile platform and the base platform and k represents the total number of joint DOF of each limb.

It is easy to know that n' is always 1 smaller than g'. For each limb, P joint provides one DOF, Qu joint provides one DOF. R joint provides one DOF and

U joint provides two DOFs. Hence, k is equal to 5. Finally, it is known that $NDOF = 3$. Hence, this PKM has 3 output motions. It should be pointed out that the 3-P (Qu) RU PKM has the 3 same main motions and 3 parasitism motions with 3-PRS PKM.

1.2 System modeling based on the double closed loop vectors method

The traditional single closed loop vector for one limb is not suited to this 3-P (Qu) RU PKM due to the complexity of its limb structure. More equations and variables should be added in its corresponding models. Hence, the double closed loop vectors method is proposed and applied in the following kinematic model, velocity model and error model.

1.2.1 Kinematic model of 3-P (Qu) RU PKM

The architecture of a 3-P (Qu) RU PKM is shown in Fig. 2. A fixed Cartesian reference coordinate system O-XYZ is fixed at the center of the base platform $B_1B_2B_3$. A moving coordinate system N-UVW is fixed at the center of the mobile platform $A_1A_2A_3$. For simplicity and without losing the generality, let the X-axis point along the direction of vector OB_1 and the U-axis point along the vector NA_1. Z-axis and W-axis are respectively perpendicular to the base platform and the mobile platform. Both axis Y and axis V satisfy the right-hand rule. B_iC_i on the base platform for $i = 1, 2$ and 3 represents the guide rail of each limb. Each P joint moves along B_iC_i. G_i is the midpoint of E_iF_i. Furthermore, all the joints attached to the base and mobile platform are symmetrically distributed at vertices of the equilateral triangles. It means that the angles on the mobile platform between vectors NA_1, NA_2 and NA_3 keep the same 2/3 π rad and the angles on the base platform between vectors OB_1, OB_2 and OB_3 keep the same 2/3 π rad no matter in 3-P (Qu) RU PKM or in 3-PRS PKM.

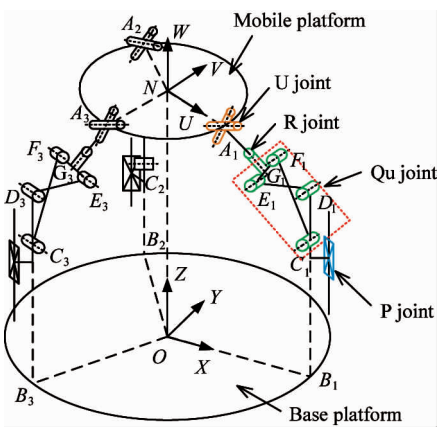

Fig. 2 Architecture of 3-P (Qu) RU PKM

In order to simplify the orientation expression, T – T rotation angle is introduced to describe the orientation of the mobile platform in both PKMs. The rotational matrix is expressed as

$$\boldsymbol{R}_{\text{T-T}} = \begin{bmatrix} \cos\varphi & -\sin\varphi & 0 \\ \sin\varphi & \cos\varphi & 0 \\ 0 & 0 & 1 \end{bmatrix} \begin{bmatrix} \cos\theta & 0 & \sin\theta \\ 0 & 1 & 0 \\ -\sin\theta & 0 & \cos\theta \end{bmatrix} \begin{bmatrix} \cos\varphi & \sin\varphi & 0 \\ -\sin\varphi & \cos\varphi & 0 \\ 0 & 0 & 1 \end{bmatrix} \begin{bmatrix} \cos\psi & -\sin\psi & 0 \\ \sin\psi & \cos\psi & 0 \\ 0 & 0 & 1 \end{bmatrix}$$

Angle ψ rotates around the normal direction of the moving platform and it is zero in an ideal situation. Furthermore, the accuracy of angle ψ is not necessary to guarantee when the machine tool machines a part. Hence, ψ can be ignored and only two angles are kept in the rotational matrix. More information about the meaning of the rotational matrix can be found in Ref. [6].

According to the above analysis, each limb has the same kinematic characteristic. The same vector loop of each limb is drown in Fig. 3. If only one closed loop vector of each limb is employed, the position of E_iF_i cannot be determined. Hence, a double closed loop vectors method ($OB_iC_iF_iG_iA_iN$ and $OB_iC_iD_iE_iG_iA_iN$) is introduced.

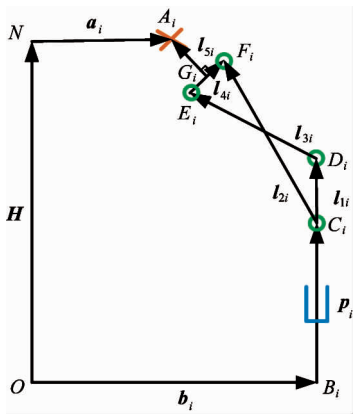

Fig. 3 The double closed loop vectors of 3-P (Qu) RU PKM

A kinematic function according to the vector loop $OB_iC_iF_iG_iA_iN$ is written as

$$\boldsymbol{H} + \boldsymbol{R}_{\text{T-T}}\boldsymbol{R}_i\boldsymbol{a}_i = \boldsymbol{R}_i\boldsymbol{b}_i + \boldsymbol{R}_i\boldsymbol{p}_i + \boldsymbol{R}_i\boldsymbol{l}_{2i} - \frac{1}{2}\boldsymbol{R}_i\boldsymbol{l}_{4i} + \boldsymbol{R}_i\boldsymbol{l}_{5i} \tag{3}$$

Another kinematic function according to the vector loop $OB_iC_iD_iE_iG_iA_iN$ is written as

$$\boldsymbol{H} + \boldsymbol{R}_{\text{T-T}}\boldsymbol{R}_i\boldsymbol{a}_i - \left(\boldsymbol{R}_i\boldsymbol{b}_i + \boldsymbol{R}_i\boldsymbol{p}_i + \boldsymbol{R}_i\boldsymbol{l}_{1i} + \frac{1}{2}\boldsymbol{R}_i\boldsymbol{l}_{4i} + \boldsymbol{R}_i\boldsymbol{l}_{5i}\right) = \boldsymbol{R}_i\boldsymbol{l}_{3i} \tag{4}$$

where $\boldsymbol{R}_i$ represents the rotation matrix of each limb. $\boldsymbol{a}_i$, $\boldsymbol{b}_i$, $\boldsymbol{l}_{1i}$, $\boldsymbol{l}_{2i}$, $\boldsymbol{l}_{3i}$, $\boldsymbol{l}_{4i}$ and $\boldsymbol{l}_{5i}$ represent the position vec-

tors of N_iA_i, O_iB_i, C_iD_i, C_iF_i, D_iE_i, E_iF_i and G_iA_i in the coordinate system O_i-$X_iY_iZ_i$, respectively. $\boldsymbol{H}$ represents the position vector of the mobile platform. p_i represents the input vector of each P joint.

The kinematic model of 3-P (Qu) RU PKM is derived based on Eqs(3) and (4). The following analyses are all based on the double closed loop vectors.

According to Eqs (3) and (4), the kinematic model is rewritten as

$$\boldsymbol{H} + \boldsymbol{R}_{\text{T-T}}\boldsymbol{R}_i\boldsymbol{a}_i - \left(\boldsymbol{R}_i\boldsymbol{b}_i + \boldsymbol{R}_i\boldsymbol{p}_i - \frac{1}{2}\boldsymbol{R}_i\boldsymbol{l}_{4i} + \boldsymbol{R}_i\boldsymbol{l}_{5i}\right) = \boldsymbol{R}_i\boldsymbol{l}_{2i} \tag{5}$$

$$\boldsymbol{H} + \boldsymbol{R}_{\text{T-T}}\boldsymbol{R}_i\boldsymbol{a}_i - \left(\boldsymbol{R}_i\boldsymbol{b}_i + \boldsymbol{R}_i\boldsymbol{p}_i + \boldsymbol{R}_i\boldsymbol{l}_{1i} + \frac{1}{2}\boldsymbol{R}_i\boldsymbol{l}_{4i} + \boldsymbol{R}_i\boldsymbol{l}_{5i}\right) = \boldsymbol{R}_i\boldsymbol{l}_{3i} \tag{6}$$

The kinematic constraint equations with the norm of both sides of Eqs(5) and (6) are expressed as

$$\left|\boldsymbol{H} + \boldsymbol{R}_{\text{T-T}}\boldsymbol{R}_i\boldsymbol{a}_i - \left(\boldsymbol{R}_i\boldsymbol{b}_i + \boldsymbol{R}_i\boldsymbol{p}_i - \frac{1}{2}\boldsymbol{R}_i\boldsymbol{l}_{4i} + \boldsymbol{R}_i\boldsymbol{l}_{5i}\right)\right| = l_2 \tag{7}$$

$$\left|\boldsymbol{H} + \boldsymbol{R}_{\text{T-T}}\boldsymbol{R}_i\boldsymbol{a}_i - \left(\boldsymbol{R}_i\boldsymbol{b}_i + \boldsymbol{R}_i\boldsymbol{p}_i + \boldsymbol{R}_i\boldsymbol{l}_{1i} + \frac{1}{2}\boldsymbol{R}_i\boldsymbol{l}_{4i} + \boldsymbol{R}_i\boldsymbol{l}_{5i}\right)\right| = l_3 \tag{8}$$

E_iF_i are fixed at G_iA_i and it is assumed that G_iA_i are perpendicular to E_iF_i. The vectors of E_iF_i and G_iA_i are expressed by one parameter ω_i as: $l_{4i} = l_4[\cos\omega_i\ 0\ \sin\omega_i]^{\text{T}}$ and $l_{5i} = l_5[\cos(\omega_i + 0.5\pi)\ 0\ \sin(\omega_i + 0.5\pi)]^{\text{T}}$. ω_i represents the orientations of E_iF_i in the X_iZ_i plane.

Considering ω_i is unknown, more expressions are needed. Multiplying both sides of Eq. (3) by $(R_ie_y)^{\text{T}}$ leads to:

$$(\boldsymbol{R}_i\boldsymbol{e}_y)^{\text{T}}(\boldsymbol{H} + \boldsymbol{R}_{\text{T-T}}\boldsymbol{R}_i\boldsymbol{a}_i) = 0 \tag{9}$$

where $\boldsymbol{e}_y = [0\ 1\ 0]^{\text{T}}$.

Based on Eqs(7) ~ (9), the kinematic model is expressed as:

$$\boldsymbol{f}_j(\boldsymbol{X}, \boldsymbol{P}, \boldsymbol{P}^*) = 0 \tag{10}$$

where $\boldsymbol{X} = [x\ y\ z\ \varphi\ \theta\ \psi]^{\text{T}}$, $\boldsymbol{P} = [p_1\ p_2\ p_3]^{\text{T}}$, $\boldsymbol{P}^* = [\omega_1\ \omega_2\ \omega_3]^{\text{T}}$, $j = 1 \sim 9$.

The double closed loop vectors method is presented above and its kinematic model is given in Eq. (10). Compared with 9 variables in the kinematic model of 3-PRS PKM, there are 12 variables in this model due to its special structure feature. The traditional single closed loop vector method for solving 9 variables is not suited to this 3-P (Qu) RU PKM and the double closed loop vectors method proposed in this paper is suitable. In this method, the 12 variables can be divided into the output and input variables. The output variable is $\boldsymbol{X}$ containing 3 main output variables and 3 parasitism output variables. The input variable is $\boldsymbol{P}$ and $\boldsymbol{P}^*$. $\boldsymbol{P}$ can be seen as the 3 main input variables and $\boldsymbol{P}^*$ can be seen as the 3 parasitism input variables. In the solving process, 3 variables are known and 9 variables are unknown. The 3 known variables correspond to the 3 main output in invers kinematics or the 3 main input in forward kinematics. Hence, no matter in invers kinematics or forward kinematics, 9 equations based on Eqs(7) ~ (9) are needed. Taking the forward kinematics as an example, it is to solve $\boldsymbol{X}$ while $\boldsymbol{P}$ is known and $\boldsymbol{P}^*$ is unknown. In order to obtain the solutions, the classical Newton iterative method is used to solve Eq. (10) as follows:

$$\boldsymbol{S}^{k+1} = \boldsymbol{S}^k - [\boldsymbol{J}(\boldsymbol{S}^k)]^{-1}\boldsymbol{F}(\boldsymbol{S}^k) \tag{11}$$

where $\boldsymbol{S}^{k+1}$ represents $\boldsymbol{X}$ and $\boldsymbol{P}^*$ in the next iterative process; and $\boldsymbol{S}^k$ is solved in the previous iterative process. $\boldsymbol{J}(\boldsymbol{S}^k)$ is the derivatives function for forward kinematics and $\boldsymbol{F}(\boldsymbol{S}^k)$ is the forward kinematics.

Starting with an initial estimate $\boldsymbol{S}^0 = [\boldsymbol{X}^0\ \ \boldsymbol{P}^{*0}]^{\text{T}}$, the iterative process will end once the following expression is satisfied:

$$\boldsymbol{S}^{k+1} - \boldsymbol{S}^k \leqslant \varepsilon \tag{12}$$

where $\boldsymbol{\varepsilon}$ is a specified tolerance.

After that, $\boldsymbol{X}$ and $\boldsymbol{P}^*$ with reference to the corresponding $\boldsymbol{P}$ are obtained.

1.2.2 Velocity model of 3-P (Qu) RU PKM

In order to obtain a velocity model, taking the derivative of Eqs(3) and (4) with respect to time, it leads to:

$$\dot{\boldsymbol{H}} + \dot{\boldsymbol{\alpha}} \times \boldsymbol{R}_{\text{T-T}}\boldsymbol{R}_i\boldsymbol{a}_i = \boldsymbol{0} + \boldsymbol{R}_i\dot{\boldsymbol{p}}_i + \boldsymbol{l}_2\dot{\boldsymbol{\omega}}_{2i} \times \boldsymbol{R}_i\boldsymbol{n}_{2i} - \frac{1}{2}\boldsymbol{R}_i\boldsymbol{l}_4\begin{bmatrix}-\sin\omega_i\\0\\\cos\omega_i\end{bmatrix}\dot{\boldsymbol{\omega}}_i + \boldsymbol{R}_i\boldsymbol{l}_{5i}\begin{bmatrix}-\cos\omega_i\\0\\-\sin\omega_i\end{bmatrix}\dot{\boldsymbol{\omega}}_i \tag{13}$$

$$\dot{\boldsymbol{H}} + \dot{\boldsymbol{\alpha}} \times \boldsymbol{R}_{\text{T-T}}\boldsymbol{R}_i\boldsymbol{a}_i = \boldsymbol{0} + \boldsymbol{R}_i\dot{\boldsymbol{p}}_i + \boldsymbol{l}_3\dot{\boldsymbol{\omega}}_{3i} \times \boldsymbol{R}_i\boldsymbol{n}_{3i} + \frac{1}{2}\boldsymbol{R}_i\boldsymbol{l}_4\begin{bmatrix}-\sin\omega_i\\0\\\cos\omega_i\end{bmatrix}\dot{\boldsymbol{\omega}}_i + \boldsymbol{R}_i\boldsymbol{l}_5\begin{bmatrix}-\cos\omega_i\\0\\-\sin\omega_i\end{bmatrix}\dot{\boldsymbol{\omega}}_i \tag{14}$$

where $\dot{\boldsymbol{H}}$ represents the position velocity vector of the output. $\dot{\boldsymbol{\alpha}}$ represents the angle velocity vector of the output. $\dot{\boldsymbol{p}}$ represents the displacement velocity vector of the inputs. $\dot{\boldsymbol{\omega}}_i$ represents the angle velocity vector of $\boldsymbol{l}_{4i}$. $\dot{\boldsymbol{\omega}}_{2i}$ and $\boldsymbol{n}_{2i}$ represent the angle velocity vector and unit direction vector of $\boldsymbol{l}_{2i}$ in X_iZ_i plane. $\dot{\boldsymbol{\omega}}_{3i}$ and $\boldsymbol{n}_{3i}$ represent the angle velocity vector and unit direction vector of $\boldsymbol{l}_{3i}$ in X_iZ_i plane.

Multiplying both sides of Eq. (13) by $(\boldsymbol{R}_i\boldsymbol{n}_{2i})^{\text{T}}$ and multiplying both sides of Eq. (14) by $(\boldsymbol{R}_i\boldsymbol{n}_{3i})^{\text{T}}$, they can be simplified as

$$\boldsymbol{S}_{hi}\dot{\boldsymbol{H}} + \boldsymbol{S}_{\alpha i}\dot{\boldsymbol{\alpha}} = S_{pi}\dot{\boldsymbol{p}}_i \tag{15}$$

Eq. (15) is rewritten as a matrix expression:

$$\boldsymbol{J}_{3\times6}\begin{bmatrix}\dot{\boldsymbol{H}}\\ \dot{\boldsymbol{\alpha}}\end{bmatrix}_{6\times1} = \dot{\boldsymbol{p}}_{3\times1} \tag{16}$$

In Eq. (16), the number of rows in $\boldsymbol{J}$ is not equal to the number of columns in $\boldsymbol{J}$. $\boldsymbol{J}$ cannot directly get a matrix inversion of itself. In order to give a further velocity analysis, the matrix of velocity transfer $\boldsymbol{J}$ should be able to be inversed. As mentioned above, this PKM has 3 main motions and 3 parasitism motions. Hence, the velocity parameters of 3 parasitism output are needed to be eliminated based on Eq. (9). By taking the derivative of Eq. (9) with respect to time, the relation between the velocity vectors of 3 main motions and 3 parasitism motions is expressed as:

$$(\boldsymbol{R}_i\boldsymbol{e}_y)^{\mathrm{T}}\dot{\boldsymbol{H}} + ((\boldsymbol{R}_{\mathrm{T\text{-}T}}\boldsymbol{R}_i\boldsymbol{a}_i)\times(\boldsymbol{R}_i\boldsymbol{e}_y))^{\mathrm{T}}\dot{\boldsymbol{\alpha}} = 0 \tag{17}$$

Eq. (17) is solved as:

$$\dot{\psi} = t_1\dot{\varphi} + t_2\dot{\theta} \tag{18}$$

Furthermore, the expressions can be obtained as

$$\dot{x} = g_1\dot{\varphi} + g_2\dot{\theta} \tag{19}$$

$$\dot{y} = g_3\dot{\varphi} + g_4\dot{\theta} \tag{20}$$

where t_1, t_2, g_1, g_2, g_3 and g_4 are the corresponding coefficients.

Taking Eqs(18) ~ (20) into Eq. (15), it leads to:

$$\begin{aligned}S_{pi}\dot{p} = {} & (S_{hix}g_1 + S_{hiy}g_3 + S_{aix} + S_{aiz}t_1)\dot{\varphi}\\ & + (S_{hix}g_2 + S_{hiy}g_4 + S_{aiy} + S_{aiz}t_2)\dot{\theta} + S_{hiz}\dot{z}\end{aligned} \tag{21}$$

Eq. (21) is rewritten as a square matrix expression:

$$[\dot{\varphi}\quad \dot{\theta}\quad \dot{z}]^{\mathrm{T}} = \boldsymbol{J}_{\mathrm{Jacobian}}[\dot{p}_1\quad \dot{p}_2\quad \dot{p}_3]^{\mathrm{T}} \tag{22}$$

1.2.3 Error model of 3-P (Qu) RU PKM

At first, Eqs(3) and (4) is taken with the first order perturbation:

$$\begin{aligned}&\boldsymbol{H} + \Delta\boldsymbol{H} + (\boldsymbol{E} + \Delta\boldsymbol{\alpha}\times)\boldsymbol{R}_{\mathrm{T\text{-}T}}\cdot\boldsymbol{R}_i\cdot(\boldsymbol{a}_i + \Delta\boldsymbol{a}_i)\\ &= \boldsymbol{R}_i\cdot(\boldsymbol{b}_i + \Delta\boldsymbol{b}_i) + \boldsymbol{R}_i\cdot(\boldsymbol{E} + \Delta\boldsymbol{\eta}_{R1i}\times)[\Delta\boldsymbol{R}_{1i}\\ &\quad + (\boldsymbol{l}_{2i} + \Delta\boldsymbol{l}_{2i})] - \frac{1}{2}\boldsymbol{R}_i\cdot(\boldsymbol{E} + \Delta\boldsymbol{\eta}_{R4i}\times)[\Delta\boldsymbol{R}_{4i}\\ &\quad + (\boldsymbol{l}_{4i} + \Delta\boldsymbol{l}_{4i})] + \boldsymbol{R}_i\cdot(\boldsymbol{p}_i + \Delta\boldsymbol{p}_i) + \boldsymbol{R}_i\cdot(\boldsymbol{l}_{5i} + \Delta\boldsymbol{l}_{5i})\\ &\quad + \boldsymbol{R}_i\cdot(\boldsymbol{E} + \Delta\boldsymbol{\eta}_{Ui}\times)\Delta\boldsymbol{U}_i\end{aligned} \tag{23}$$

$$\begin{aligned}&\boldsymbol{H} + \Delta\boldsymbol{H} + (\boldsymbol{E} + \Delta\boldsymbol{\alpha}\times)\boldsymbol{R}_{\mathrm{T\text{-}T}}\cdot\boldsymbol{R}_i\cdot(\boldsymbol{a}_i + \Delta\boldsymbol{a}_i)\\ &= \boldsymbol{R}_i\cdot(\boldsymbol{b}_i + \Delta\boldsymbol{b}_i) + \boldsymbol{R}_i\cdot(\boldsymbol{p}_i + \Delta\boldsymbol{p}_i) + \boldsymbol{R}_i\cdot(\boldsymbol{l}_{1i} + \Delta\boldsymbol{l}_{1i})\\ &\quad + \boldsymbol{R}_i\cdot(\boldsymbol{E} + \Delta\boldsymbol{\eta}_{R2i}\times)[\Delta\boldsymbol{R}_{2i} + (\boldsymbol{l}_{3i} + \Delta\boldsymbol{l}_{3i})]\\ &\quad + \frac{1}{2}\boldsymbol{R}_i\cdot(\boldsymbol{E} + \Delta\boldsymbol{\eta}_{R3i}\times)[\Delta\boldsymbol{R}_{3i} + (\boldsymbol{l}_{4i} + \Delta\boldsymbol{l}_{4i})]\\ &\quad + \boldsymbol{R}_i\cdot(\boldsymbol{l}_{5i} + \Delta\boldsymbol{l}_{5i}) + \boldsymbol{R}_i\cdot(\boldsymbol{E} + \Delta\boldsymbol{\eta}_{Ui}\times)\Delta\boldsymbol{U}_i\end{aligned} \tag{24}$$

where $\Delta\boldsymbol{H}$ represents the position error vector of the output; $\Delta\boldsymbol{\alpha}$ represents the orientation error vector of the output; $\Delta\boldsymbol{a}_i$ represents the error vector of $\boldsymbol{a}_i$. $\Delta\boldsymbol{b}_i$represents the error vector of $\boldsymbol{b}_i$. $\Delta\boldsymbol{p}_i$ represents the error vector of $\boldsymbol{p}_i$. $\Delta\boldsymbol{l}_{mi}$ represents the error vector of $\boldsymbol{l}_{mi}$ for $m = 1$ to 5; $\Delta\boldsymbol{\eta}_{R1i}$, $\Delta\boldsymbol{\eta}_{R2i}$, $\Delta\boldsymbol{\eta}_{R3i}$ and $\Delta\boldsymbol{\eta}_{R4i}$ represent the orientation error vector of four R joints of Qu joint. $\Delta\boldsymbol{R}_{1i}$, $\Delta\boldsymbol{R}_{2i}$, $\Delta\boldsymbol{R}_{3i}$ and $\Delta\boldsymbol{R}_{4i}$ represent the position error vector of four R joints of Qu joint; $\Delta\boldsymbol{\eta}_{Ui}$ represents the orientation error vector of U joint; $\Delta\boldsymbol{U}_i$ represents the position error vector of U joint. Furthermore, it should be pointed out that the R joint connecting E_iF_i with G_iA_i can be ignored because the main error of the R joint is the rotational motion around its normal direction and it cannot influence the error of the mobile platform.

With ignoring the second and higher order terms, Eq. (23) is subtracted from Eq. (3) and Eq. (24) is subtracted from Eq. (4):

$$\begin{aligned}&\Delta\boldsymbol{H} + \Delta\boldsymbol{\alpha}\times\boldsymbol{R}_{\mathrm{T\text{-}T}}\boldsymbol{R}_i\boldsymbol{a}_i\\ &= -\boldsymbol{R}_{\mathrm{T\text{-}T}}\boldsymbol{R}_i\Delta\boldsymbol{a}_i + \boldsymbol{R}_i\Delta\boldsymbol{b}_i + \boldsymbol{R}_i\Delta\boldsymbol{p}_i + \boldsymbol{R}_i\Delta\boldsymbol{R}_{1i} + \boldsymbol{R}_i\Delta\boldsymbol{l}_{2i}\\ &\quad + \boldsymbol{R}_i\Delta\boldsymbol{\eta}_{R1i}\times\boldsymbol{l}_{2i} - \frac{1}{2}(\boldsymbol{R}_i\Delta\boldsymbol{R}_{4i} + \boldsymbol{R}_i\Delta\boldsymbol{l}_{4i} + \boldsymbol{R}_i\Delta\boldsymbol{\eta}_{R4i}\\ &\quad \times\boldsymbol{l}_{4i}) + \boldsymbol{R}_i\Delta\boldsymbol{U}_i + \boldsymbol{R}_i\Delta\boldsymbol{l}_{5i}\end{aligned} \tag{25}$$

$$\begin{aligned}&\Delta\boldsymbol{H} + \Delta\boldsymbol{\alpha}\times\boldsymbol{R}_{\mathrm{T\text{-}T}}\boldsymbol{R}_i\boldsymbol{a}_i\\ &= -\boldsymbol{R}_{\mathrm{T\text{-}T}}\boldsymbol{R}_i\Delta\boldsymbol{a}_i + \boldsymbol{R}_i(\Delta\boldsymbol{b}_i + \Delta\boldsymbol{p}_i + \Delta\boldsymbol{l}_{1i} + \Delta\boldsymbol{R}_{2i} + \Delta\boldsymbol{l}_{3i})\\ &\quad + \boldsymbol{R}_i\Delta\boldsymbol{\eta}_{R2i}\times\boldsymbol{l}_{3i} + \frac{1}{2}(\boldsymbol{R}_i\Delta\boldsymbol{R}_{3i} + \boldsymbol{R}_i\Delta\boldsymbol{l}_{4i} + \boldsymbol{R}_i\Delta\boldsymbol{\eta}_{R3i}\\ &\quad \times\boldsymbol{l}_{4i}) + \boldsymbol{R}_i\Delta\boldsymbol{U}_i + \boldsymbol{R}_i\Delta\boldsymbol{l}_{5i}\end{aligned} \tag{26}$$

Multiplying both sides of Eq. (25) by $(\boldsymbol{R}_i\boldsymbol{e}_y)^{\mathrm{T}}$ and multiplying both sides of Eq. (26) by $(\boldsymbol{R}_i\boldsymbol{l}_{3i})^{\mathrm{T}}$, they lead to:

$$\begin{aligned}&(\boldsymbol{R}_i\boldsymbol{e}_y)^{\mathrm{T}}\cdot\Delta\boldsymbol{H} + [(\boldsymbol{R}_{\mathrm{T\text{-}T}}\boldsymbol{R}_i\boldsymbol{a}_i)\times(\boldsymbol{R}_i\boldsymbol{e}_y)]^{\mathrm{T}}\cdot\Delta\boldsymbol{\alpha}\\ &= (\boldsymbol{R}_i\boldsymbol{e}_y)^{\mathrm{T}}\cdot(-\boldsymbol{R}_{\mathrm{T\text{-}T}}\boldsymbol{R}_i\Delta\boldsymbol{a}_i + \boldsymbol{R}_i\Delta\boldsymbol{b}_i + \boldsymbol{R}_i\Delta\boldsymbol{p}_i + \boldsymbol{R}_i\Delta\boldsymbol{R}_{1i}\\ &\quad + \boldsymbol{R}_i\Delta\boldsymbol{l}_{2i}) + (\boldsymbol{l}_{2i}\times\boldsymbol{e}_y)^{\mathrm{T}}\cdot\Delta\boldsymbol{\eta}_{R1i} - \frac{1}{2}(\boldsymbol{R}_i\boldsymbol{e}_y)^{\mathrm{T}}\\ &\quad \cdot(\boldsymbol{R}_i\Delta\boldsymbol{R}_{4i} + \boldsymbol{R}_i\Delta\boldsymbol{l}_{4i}) - \frac{1}{2}(\boldsymbol{l}_{4i}\times\boldsymbol{e}_y)^{\mathrm{T}}\cdot\Delta\boldsymbol{\eta}_{R4i}\\ &\quad + (\boldsymbol{R}_i\boldsymbol{e}_y)^{\mathrm{T}}\cdot(\boldsymbol{R}_i\Delta\boldsymbol{U}_i + \boldsymbol{R}_i\Delta\boldsymbol{l}_{5i})\end{aligned} \tag{27}$$

$$\begin{aligned}&(\boldsymbol{R}_i\boldsymbol{l}_{3i})^{\mathrm{T}}\Delta\boldsymbol{H} + [(\boldsymbol{R}_{\mathrm{T\text{-}T}}\boldsymbol{R}_i\boldsymbol{a}_i)\times(\boldsymbol{R}_i\boldsymbol{l}_{3i})]^{\mathrm{T}}\Delta\boldsymbol{\alpha}\\ &= (\boldsymbol{R}_i\boldsymbol{l}_{3i})^{\mathrm{T}}(-\boldsymbol{R}_{\mathrm{T\text{-}T}}\boldsymbol{R}_i\Delta\boldsymbol{a}_i + \boldsymbol{R}_i(\Delta\boldsymbol{b}_i + \Delta\boldsymbol{p}_i + \Delta\boldsymbol{l}_{1i} + \Delta\boldsymbol{R}_{2i}))\\ &\quad + (\boldsymbol{l}_{3i}\times\boldsymbol{l}_{3i})^{\mathrm{T}}\Delta\boldsymbol{\eta}_{R2i} + \frac{1}{2}(\boldsymbol{R}_i\boldsymbol{l}_{3i})^{\mathrm{T}}(\boldsymbol{R}_i\Delta\boldsymbol{R}_{3i} + \boldsymbol{R}_i\Delta\boldsymbol{l}_{4i})\\ &\quad + \frac{1}{2}(\boldsymbol{l}_{4i}\times\boldsymbol{l}_{3i})^{\mathrm{T}}\Delta\boldsymbol{\eta}_{R3i} + (\boldsymbol{R}_i\boldsymbol{l}_{3i})^{\mathrm{T}}(\boldsymbol{R}_i\Delta\boldsymbol{U}_i + \boldsymbol{R}_i\Delta\boldsymbol{l}_{5i}\\ &\quad + \boldsymbol{R}_i\Delta\boldsymbol{l}_{3i})\end{aligned} \tag{28}$$

Then the expression of the error model based on Eqs(27) and (28) can be written as:

$$\boldsymbol{J}_{\mathrm{error}}\begin{bmatrix}\Delta\boldsymbol{H}\\ \Delta\boldsymbol{\alpha}\end{bmatrix} = \Delta\boldsymbol{p} \tag{29}$$

where $\Delta\boldsymbol{P}$ represents a vector with all error parameters of 3-P (Qu) RU PKM.

2 System modeling of 3-PRS PKM

Since the 3-PRS PKM has been analyzed by sev-

eral researches, its kinematic model, velocity model and error model are briefly introduced. Its architecture is presented in Fig. 4. The 3-PRS PKM is also composed of a mobile platform, a base platform and 3 supporting limbs with the identical kinematics. The base platform is connected with the mobile platform by each limb containing one P joint, one R joint and one S joint. In addition, P joint on each limb is actuated. The 3-PRS PKM has the 3 same main motions and 3 parasitism motions with the 3-P (Qu) RU PKM.

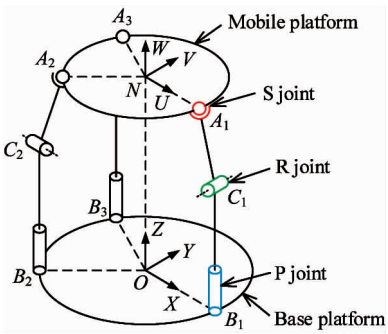

Fig. 4 Architecture of 3-PRS PKM

In order to compare the two PKMs in convenience, a same naming rule is employed to describe the 3-PRS PKM in Fig. 4. A fixed Cartesian reference coordinate system O-XYZ is fixed at the center of the base platform $B_1B_2B_3$. A moving Cartesian reference coordinate system N-UVW is fixed at the center of the mobile platform $A_1A_2A_3$. For simplicity and without losing the generality, let the X-axis point along the direction of vector OB_1 and the U-axis point along vector NA_1. Z-axis and W-axis are respectively perpendicular to the base platform and the mobile platform. Both Y-axis and V-axis satisfy the right-hand rule. B_iC_i on the base platform for $i = 1$, 2 and 3 represents the guide rail of each limb. The guide rail of each limb is perpendicular to the base platform. Each P joint moves along B_iC_i.

Some expressions and introductions mentioned in the model of 3-P (Qu) RU PKM are not presented again in this section.

A kinematic model according to vector loop $OB_iC_iA_iN$ is written as:

$$\boldsymbol{H} + \boldsymbol{R}_{\text{T-T}}\boldsymbol{R}_i\boldsymbol{a}_i = \boldsymbol{R}_i\boldsymbol{b}_i + \boldsymbol{R}_i\boldsymbol{p}_i + \boldsymbol{R}_i\boldsymbol{l}_i \tag{30}$$

By taking the derivative of Eq. (30) with respect to time, the velocity model is written as:

$$\dot{\boldsymbol{H}} + \dot{\boldsymbol{\alpha}} \times \boldsymbol{R}_{\text{T-T}}\boldsymbol{R}_i\boldsymbol{a}_i = \boldsymbol{0} + \dot{\boldsymbol{p}}_i\boldsymbol{R}_i\boldsymbol{e}_z + l\xi_i \times \boldsymbol{n}_{li} \tag{31}$$

where ξ_i represents the angle velocity vector of l_i and n_{li} represents the unit direction vector of l_i.

Multiplying both sides of Eq. (31) by $(\boldsymbol{n}_{li})^{\text{T}}$, it leads to:

$$\boldsymbol{n}_{li}^{\text{T}}\dot{\boldsymbol{H}} + (\boldsymbol{R}_{\text{T-T}}\boldsymbol{R}_i\boldsymbol{a}_i \times \boldsymbol{n}_{li})^{\text{T}}\dot{\boldsymbol{\alpha}} = \dot{\boldsymbol{p}}_i\boldsymbol{n}_{li}^{\text{T}}\boldsymbol{R}_i\boldsymbol{e}_z \tag{32}$$

Eq. (32) can be rewritten in the same matrix-format with Eq. (22):

$$[\dot{\varphi} \quad \dot{\theta} \quad \dot{z}]^{\text{T}} = \boldsymbol{J}_{\text{Jacobian}}[\dot{p}_1 \quad \dot{p}_2 \quad \dot{p}_3]^{\text{T}} \tag{33}$$

The error model of 3-PRS PKM is given directly:

$$\begin{aligned}(\boldsymbol{R}_i\boldsymbol{l}_i)^{\text{T}}\Delta\boldsymbol{H} + [(\boldsymbol{R}_{\text{T-T}}\boldsymbol{R}_i\boldsymbol{a}_i) \times (\boldsymbol{R}_i\boldsymbol{l}_i)]^{\text{T}}\Delta\boldsymbol{\alpha} \\ = (\boldsymbol{R}_i\boldsymbol{l}_i)^{\text{T}}(-\boldsymbol{R}_{\text{T-T}}\boldsymbol{R}_i\Delta\boldsymbol{a}_i + \boldsymbol{R}_i\Delta\boldsymbol{b}_i + \boldsymbol{R}_i\Delta\boldsymbol{p}_i) \\ + (\boldsymbol{R}_i\boldsymbol{l}_i)^{\text{T}}(\boldsymbol{R}_i\Delta\boldsymbol{R}_i + \boldsymbol{R}_i\Delta\boldsymbol{l}_i + \boldsymbol{R}_i\Delta\boldsymbol{S}_i) \\ + (\boldsymbol{l}_i \times \boldsymbol{l}_i)^{\text{T}}\Delta\boldsymbol{\eta}_{Ri}\end{aligned} \tag{34}$$

$$\begin{aligned}(\boldsymbol{R}_i\boldsymbol{e}_y)^{\text{T}}\Delta\boldsymbol{H} + [(\boldsymbol{R}_{\text{T-T}}\boldsymbol{R}_i\boldsymbol{a}_i) \times (\boldsymbol{R}_i\boldsymbol{e}_y)]^{\text{T}}\Delta\boldsymbol{\alpha} \\ = (\boldsymbol{R}_i\boldsymbol{e}_y)^{\text{T}}(-\boldsymbol{R}_{\text{T-T}}\boldsymbol{R}_i\Delta\boldsymbol{a}_i + \boldsymbol{R}_i\Delta b_i + \boldsymbol{R}_i\Delta\boldsymbol{p}_i) \\ + (\boldsymbol{R}_i\boldsymbol{e}_y)^{\text{T}}(\boldsymbol{R}_i\Delta\boldsymbol{R}_i + \boldsymbol{R}_i\Delta\boldsymbol{l}_i + \boldsymbol{R}_i\Delta\boldsymbol{S}_i) \\ + (\boldsymbol{l}_i \times \boldsymbol{e}_y)^{\text{T}}\Delta\boldsymbol{\eta}_{Ri}\end{aligned} \tag{35}$$

where $\Delta\boldsymbol{l}_i$ represents the error vector of $\boldsymbol{l}_i$; $\Delta\boldsymbol{\eta}_{Ri}$ represents the orientation error vector of R joints; $\Delta\boldsymbol{R}_i$ represents the position error vector of R joint; $\Delta\boldsymbol{S}_i$ represents the position error vector of S joint.

Furthermore, the error model of 3-PRS PKM is also obtained in the same format with Eq. (29) as:

$$\boldsymbol{J}_{\text{error}}\begin{bmatrix}\Delta\boldsymbol{H} \\ \Delta\boldsymbol{\alpha}\end{bmatrix} = \Delta\boldsymbol{p} \tag{36}$$

where $\Delta\boldsymbol{P}$ represents a vector with all error parameters of 3-PRS PKM.

3 Performance evaluation indices

To be fair, the structure parameters of 3-P (Qu) RU PKM are given based on the structure parameters of 3-PRS PKM. Two rules are set up:

1) Keep $\boldsymbol{a}_i$ and $\boldsymbol{b}_i$ of both PKMs in the same-lengths;

2) At $\varphi = 0$ and $\theta = 0$, the structure parameters of both the two PKMs should satisfy the following expressions:

$$\frac{1}{2}\boldsymbol{l}_{1i} + \boldsymbol{l}_i = \boldsymbol{l}_{2i} - \frac{1}{2}\boldsymbol{l}_{4i} + \boldsymbol{l}_{5i} \tag{37}$$

$$\frac{1}{2}\boldsymbol{l}_{1i} + \boldsymbol{l}_i = \boldsymbol{l}_{1i} + \boldsymbol{l}_{3i} + \frac{1}{2}\boldsymbol{l}_{4i} + \boldsymbol{l}_{5i} \tag{38}$$

According to the above rules, all the structure parameters of 3-P (Qu) RU PKM can be obtained with the structure parameters of 3-PRS PKM and the given lengths of $\boldsymbol{l}_{1i}$, $\boldsymbol{l}_{4i}$ and $\boldsymbol{l}_{5i}$. After calculating Eqs(37) and (38), the structure parameters of both PKMs are given in the following. In 3-PRS PKM, $a = 200$mm, $b = 260$mm and $l = 460$mm. In 3-P (Qu) RU PKM, $a = 200$mm, $b = 260$mm, $l_1 = 240$mm, $l_2 = 533$mm, $l_3 = 293$mm, $l_4 = 100$mm and $l_5 = 50$mm.

3.1 Workspace

In order to evaluate the workspace performance, an index is introduced.

$$\lambda(X) = | \boldsymbol{q}_{x\max} - \boldsymbol{q}_{x\min} | \tag{39}$$

where $\boldsymbol{q}_{x\max}$ represents an output point containing the maximum value along $\boldsymbol{X}$ direction. $\boldsymbol{q}_{x\min}$ represents an output point containing the minimum value along $\boldsymbol{X}$ direction. To put this conveniently, $\lambda(\boldsymbol{X})$ is represented by *DAXD* (distance along *X*direction).

The same operations are performed along *Y* direction and *Z* direction. *DAYD* and *DAZD* respectively represent the distances along *Y* direction and *Z* direction. The bigger *DAXD*, *DAYD* and *DAZD* are, the bigger workspace the PKM has.

3.2 Manipulator dexterity

The character of the velocity transfer matrix for a PKM is seen as the ability to change the positions and orientations of the mobile platform. One of the frequently used indices based on the velocity transfer matrix is called dexterity. A dexterity index for a given output point is $1/\kappa$. κ represents the condition number of the velocity transfer matrix for 3-P (Qu) RU PKM in Eq. (22) or for 3-PRS PKM in Eq. (33). The condition number κ ranges from 1 to ∞. For a given output point which κ is equal to 1, it means that the dexterity of the PKM is the best and the PKM is isotropic. Furthermore, *GDI* (global dexterity index) is given to evaluate both PKMs in a given output range:

$$\mu = \frac{\int_V (1/\kappa)\,\mathrm{d}V}{V} \tag{40}$$

where μ represents a value of *GDI*, *V* denotes a given output rang. The bigger μ is, the better the velocity performance the PKM has.

3.3 Position error

Although PKMs own many merits such as high speed and heavy load handling, the accuracy performance should be paid attentions to if a PKM is used as a tool head. Position error of a PKM is an important evaluation index of the accuracy performance. A determination of the position errors for a given output point is put forward in the following:

$$\Omega_{\mathrm{H}} = | \Delta \boldsymbol{H} | \tag{41}$$

where Ω_{H} represents the position error. $\Delta \boldsymbol{H}$ for 3-P (Qu) RU PKM is calculated by Eq. (29) and one for 3-PRS PKM is calculated by Eq. (36). The bigger the value of Ω_{H} is, the worse accuracy the PKM has.

3.4 Error sensitivity

The position error is influenced by the values of the given structural errors, which cannot comprehensively reflect the accuracy performance of a PKM. Error sensitivity is employed to estimate the influence of all error parameters on the output error. A determination of a global position error sensitivity for a given output range is put forward in the following:

$$\sigma_H = \frac{\int_V \sqrt{\left[\frac{\partial(\Delta H_x)}{\partial(\Delta p_H)}\right]^2 + \left[\frac{\partial(\Delta H_y)}{\partial(\Delta p_H)}\right]^2 + \left[\frac{\partial(\Delta H_z)}{\partial(\Delta p_H)}\right]^2}\,\mathrm{d}V}{V} \tag{42}$$

where *V* denotes a given output range. ΔH_x, ΔH_y and ΔH_z respectively represent elements of the position output error vector. ΔP_H represents the unit position error parameter of a joint. σ_{H} presents the influence of a unit error of a joint position error parameter on the position error of the output error.

Furthermore, the position error sensitivity and orientation error sensitivity should be discussed respectively. The similar determination of a global orientation error sensitivity for a given output range is also proposed:

$$\sigma_\alpha = \frac{\int_V \sqrt{\left[\frac{\partial(\Delta \alpha_x)}{\partial(\Delta p_\alpha)}\right]^2 + \left[\frac{\partial(\Delta \alpha_y)}{\partial(\Delta p_\alpha)}\right]^2 + \left[\frac{\partial(\Delta \alpha_z)}{\partial(\Delta p_\alpha)}\right]^2}\,\mathrm{d}V}{V} \tag{43}$$

where $\Delta\alpha_x$, $\Delta\alpha_y$ and $\Delta\alpha_z$ respectively represent elements of the orientation output error vector. ΔP_α represents the unit orientation error parameter of a joint. σ_α presents the influence of a unit error of a joint orientation error parameter on the orientation error of the output error.

The error sensitivity reflects the influence of a unit error of a joint on the output error. This index estimates the influence of each single joint error on the output error rather than the influence of all joints error together on the output error. The bigger the error sensitivity is, the worse accuracy the PKM has.

4 Numerical examples

Based on the above evaluation indices, numerical examples are employed to show specific performances between the 3-P (Qu) RU PKM and 3-PRS PKM on workspace, manipulator dexterity, position error and error sensitivity.

4.1 Workspace comparison

In this section, kinematic workspaces of both PKMs are obtained with the same input range. Both of the PKMs own the same motion boundary on workspace. Moreover, it is seen that workspaces of both PKMs are totally the same since the values of *DAXD*, *DAYD* and *DAZD* are the same as 46mm, 37mm and

100mm, respectively. Collections of every dispersed output point for both PKMs are plotted in Fig. 5. The comparison result reveals that this 3-P (Qu) RU PKM owns the same kinematic workspace with a 3-PRS PKM, which ensures a basic machining trajectory requirement for a tool head.

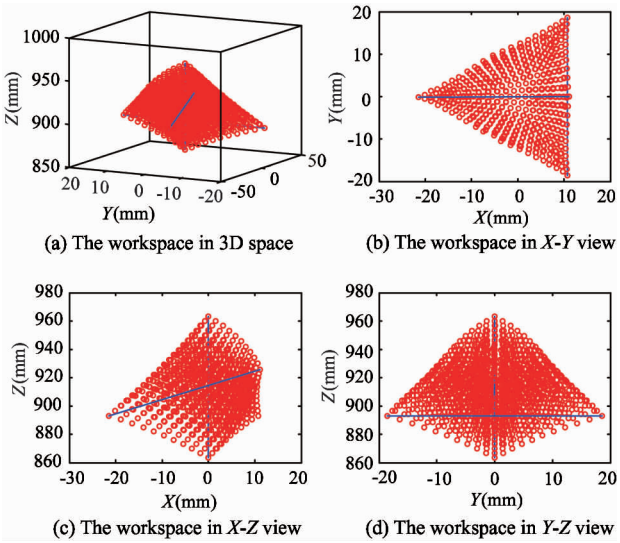

Fig. 5 The workspace of both PKMs

4.2 Dexterity comparison

The dexterity index of each PKM is calculated at each output points in a given output range with $Z = 700$mm, $\varphi = 0 \sim 2\pi$ and $\theta = 0 \sim \pi/4$. In order to present the dexterity of each PKM comprehensively, the dexterity distributions respectively along three DOF directions are given. Their specific situations are Z DOF varying in 600mm to 800mm with $\varphi = 0$ and $\theta = \pi/6$, φ DOF varying in 0 to 2π with $Z = 700$mm and $\theta = \pi/6$, θ DOF varying in 0 to $\pi/4$ with $Z = 700$mm and $\varphi = 0$. Distributions of dexterity index for 3-P (Qu) RU PKM and 3-PRS PKM are respectively plotted in Fig. 6.

It shows that both of the two PKMs present a similar dexterity distribution. The big values of dexterity index are both in the center and some specific edges of the given output range. Moreover, the biggest *GDI* value of the 3-PRS PKM is 0.0068 and smaller than that of the 3-P (Qu) RU PKM, being 0.0126, which means that the manipulator dexterity performance of the 3-P (Qu) RU PKM is better. According to the meaning of manipulator dexterity, the 3-P (Qu) RU PKM owns a better isotropic motion and performs well with regard to its force and motion transmission capability. Hence, it can be concluded that the 3-P (Qu) RU PKM has more advantages in the aspect of manipulator dexterity.

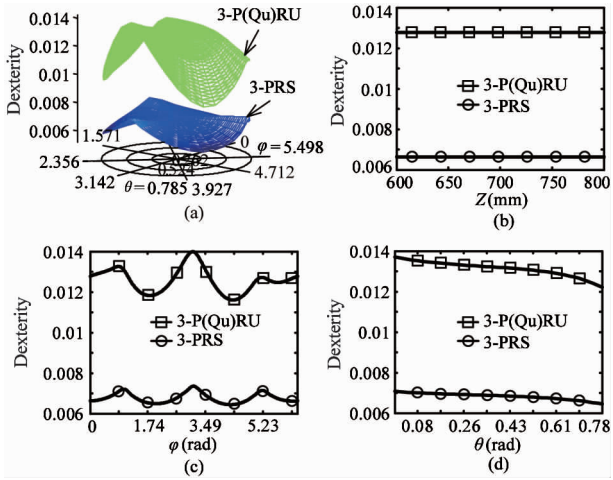

(a) $Z = 700$mm, $\varphi = 0 \sim 2\pi$ and $\theta = 0 \sim \pi/4$; (b) Z DOF varying in 600mm to 800mm with $\varphi = 0$ and $\theta = \pi/6$; (c) φ DOF varying in 0 to 2π with $Z = 700$mm and $\theta = \pi/6$; (d) θ DOF varying in 0 to $\pi/4$ with $Z = 700$mm and $\varphi = 0$

Fig. 6 Distributions of dexterity for 3-P (Qu) RU PKM and 3-PRS PKM

4.3 Position error comparison

In order to obtain a fair error comparison between the two PKMs, errors of the common structural parameters are kept in the same. Structural errors of the 3-P (Qu) RU PKM and the 3-PRS PKM are given in random within a given range. The position error simulations of the two PKMs are performed in the same range with Section 4.2.

Fig. 7 and Fig. 8 show that both of the two PKMs present a similar position error distribution. The big values of position error are both at some specific edges of the given output range. Furthermore, the maximum values of position errors of the 3-P (Qu) RU PKM and

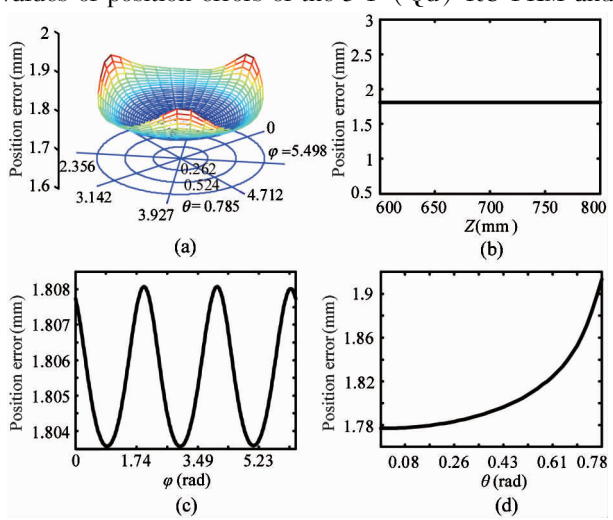

(a) $Z = 700$mm, $\varphi = 0 \sim 2\pi$ and $\theta = 0 \sim \pi/4$; (b) Z DOF varying in 600mm to 800mm with $\varphi = 0$ and $\theta = \pi/6$; (c) φ DOF varying in 0 to 2π with $Z = 700$mm and $\theta = \pi/6$; (d) θ DOF varying in 0 to $\pi/4$ with $Z = 700$mm and $\varphi = 0$

Fig. 7 Position errors of 3-P (Qu) RU PKM

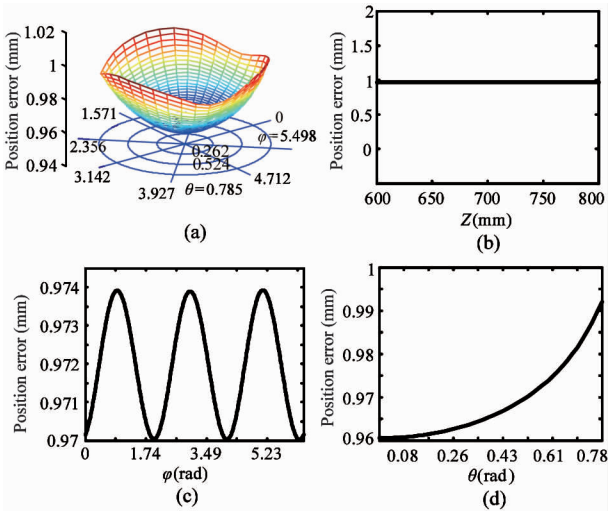

(a) $Z=700$mm, $\varphi=0\sim2\pi$ and $\theta=0\sim\pi/4$; (b) Z DOF varying in 600mm to 800mm with $\varphi=0$ and $\theta=\pi/6$; (c) φ DOF varying in 0 to 2π with $Z=700$mm and $\theta=\pi/6$; (d) θ DOF varying in 0 to $\pi/4$ with $Z=700$mm and $\varphi=0$

Fig. 8 Position errors of 3-PRS PKM

the 3-PRS PKM are 1.919mm and 1.002mm respectively. The data show that the position error of the 3-P (Qu) RU PKM is bigger than that of the 3-PRS PKM. It reveals that the 3-PRS PKM is better than the 3-P (Qu) RU PKM in the aspect of position errors.

4.4 Error sensitivity comparison

The difference between the two PKMs is the joints. Qu joint (including four R joints), R joint and U joint of the 3-P (Qu) RU PKM are different from R joint and S joint of the 3-PRS PKM. P joints of both PKMs are totally the same. In the following discussions, just the different joints are analyzed. As mentioned above in Section 1.2.3, the R joint of the 3-P (Qu) RU PKM is ignored. Hence, the error sensitivity of Qu joint (four R joints) and U joint of the 3-P (Qu) RU PKM are compared with R joint and S joint of the 3-PRS PKM. The simulation results of error sensitivities based on the global range and 4 poses are given in Tables 1 and 2. The global range is $Z=700$mm, $\varphi=0\sim2\pi$ and $\theta=0\sim\pi/4$. The 4 poses are $Z=700$mm, $\varphi=0$ and $\theta=\pi/6$, $Z=700$mm, $\varphi=\pi/2$and $\theta=\pi/6$, $Z=700$mm, $\varphi=\pi$ and $\theta=\pi/6$ and $Z=700$mm, $\varphi=3\pi/2$ and $\theta=\pi/6$, respectively.

It is found that the biggest global position error sensitivity values of the two PKMs are both about 0.7 and the biggest global orientation error sensitivity values of the two PKMs are both about 0.35. The global error sensitivity of both the two PKMs keep in a similar level. It reveals that the unit error of each joint of both PKMs has a similar influence on the output error. However, the 3-P (Qu) RU PKM is worse than the 3-PRS PKM in the aspect of position errors based on the same structural errors. It can be thought that bigger output error value of the 3-P (Qu) RU PKM is caused by a

Table 1 Error sensitivity of 3-P (Qu) RU PKM with different poses

Joint	Global	Pose 1	Pose 2	Pose 3	Pose 4
ΔR_{1ix}	0	0	0	0	0
ΔR_{1iy}	0.6771	0.6591	0.6506	0.7288	0.6506
ΔR_{1iz}	0	0	0	0	0
ΔR_{2ix}	0.0889	0.1499	0.0523	0.1034	0.0523
ΔR_{2iy}	0	0	0	0	0
ΔR_{2iz}	0.3840	0.4714	0.3731	0.3251	0.3731
ΔR_{3ix}	0.0444	0.0749	0.0261	0.0517	0.0261
ΔR_{3iy}	0	0	0	0	0
ΔR_{3iz}	0.1920	0.2357	0.1865	0.1625	0.1865
ΔR_{4ix}	0	0	0	0	0
ΔR_{4iy}	0.3385	0.3295	0.3253	0.3644	0.3253
ΔR_{4iz}	0	0	0	0	0
ΔU_{ix}	0.0889	0.1499	0.0523	0.1034	0.0523
ΔU_{iy}	0.6771	0.6591	0.6506	0.7288	0.6506
ΔU_{iz}	0.3840	0.4714	0.3731	0.3251	0.3731
$\Delta\eta_{R1ix}$	0.3928	0.3812	0.3783	0.4215	0.3783
$\Delta\eta_{R1iy}$	0	0	0	0	0
$\Delta\eta_{R1iz}$	0.0162	0.0342	0.0017	0.0378	0.0017
$\Delta\eta_{R2ix}$	0	0	0	0	0
$\Delta\eta_{R2iy}$	0	0	0	0	0
$\Delta\eta_{R2iz}$	0.0001	0.0002	0.0001	0.0001	0.0001
$\Delta\eta_{R3ix}$	0	0.0001	0	0.0001	0
$\Delta\eta_{R3iy}$	0	0	0	0	0
$\Delta\eta_{R3iz}$	0.0003	0.0004	0.0003	0.0003	0.0003
$\Delta\eta_{R4ix}$	0.0072	0.0099	0.0045	0.0110	0.0045
$\Delta\eta_{R4iy}$	0	0	0	0	0
$\Delta\eta_{R4iz}$	0.0329	0.0314	0.0322	0.0347	0.0322

Table 2 Error sensitivity of 3-PRS PKM with different poses

Joint	Global	Pose 1	Pose 2	Pose 3	Pose 4
ΔR_{ix}	0.0611	0.0982	0.0385	0.0759	0.0385
ΔR_{iy}	0.6712	0.667	0.6467	0.7178	0.6467
ΔR_{iz}	0.3777	0.4416	0.3756	0.3411	0.3756
ΔS_{ix}	0.0611	0.0982	0.0385	0.0759	0.0385
ΔS_{iy}	0.6712	0.667	0.6467	0.7178	0.6467
ΔS_{iz}	0.3777	0.4416	0.3756	0.3411	0.3756
$\Delta\eta_{ix}$	0.3046	0.2995	0.2959	0.3223	0.2959
$\Delta\eta_{iy}$	0	0	0	0	0
$\Delta\eta_{iz}$	0.0481	0.0666	0.0303	0.0717	0.0303

plenty of joints. Hence, the 3-P (Qu) RU PKM containing more joints is worse than the 3-PRS PKM in the aspect of position errors. From the aspect of error sensitivity, it can be seen that accuracy performance of these two PKMs are basically on a similar level.

5 Conclusion

In this paper, a novel symmetrical 3-DOF PKM, named 3-P (Qu) RU, is firstly presented and investigated. According to its structure feature, a double closed loop vectors method is proposed to establish its kinematic model, velocity transfer model and error model. In order to show the performance of the 3-P (Qu) RU PKM, a comparison study of numerical simulations with a 3-PRS PKM is presented. The results reveal that this 3-P (Qu) RU PKM owns the same kinematic workspace with the 3-PRS PKM. And it owns a better isotropic motion and performs well with regard to its force and motion transmission capability. However, it is found that the 3-P (Qu) RU PKM has a bigger output error value but keeps the similar level in the aspect of error sensitivity with the 3-PRS PKM. In general, the accuracy performance of 3-P (Qu) RU PKM is worse than that of 3-PRS PKM.

Compare with the 3-PRS PKM which is applied in the 5-axis hybrid machine tool successfully, it shows that the 3-P (Qu) RU PKM has potential applications in the field of hybrid machine tools. In order to develop the 3-P (Qu) RU PKM in practice, its accuracy performance should be improved by other further studies, including the accuracy design and kinematic calibration method. This paper gives an available selection for a tool head of a hybrid machine tool and the analysis in this paper is greatly helpful for further applications of the 3-P (Qu) RU PKM.

References

[1] Yang G, Chen I M, Chen W, et al. Kinematic design of a six-DOF parallel-kinematics machine with decoupled-motion architecture. *IEEE Transactions on Robotics*, 2004, 20(5): 876-887

[2] Wu J, Chen X, Wang L, et al. Dynamic load-carrying capacity of a novel redundantly actuated parallel conveyor. *Nonlinear Dynamics*, 2014, 78(1): 241-250

[3] Pandilov Z, Rall K. Parallel kinematics machine tools: history, present, future. *Mechanical Engineering-Scientific Journal*, 2006, 25(1): 3-20

[4] Zhang D, Gosselin C M. Kinetostatic analysis and design optimization of the tricept machine tool family. *Journal of Manufacturing Science and Engineering*, 2002, 124(3): 725-733

[5] Huang T, Li M, Zhao X M, et al. Conceptual design and dimensional synthesis for a 3-DOF module of the TriVariant-a novel 5-DOF reconfigurable hybrid robot. *IEEE Transactions on Robotics*, 2005, 21(3): 449-456

[6] Xie F, Liu X J, Wang J. A 3-DOF parallel manufacturing module and its kinematic optimization. *Robotics and Computer-Integrated Manufacturing*, 2012, 28(3): 334-343

[7] Bonnemains T, Chanal H, Bouzgarrou B C, et al. Dynamic model of an overconstrained PKM with compliances: The Tripteor X7. *Robotics and Computer-Integrated Manufacturing*, 2013, 29(1): 180-191

[8] Gojtan G E E, Furtado G P, Hess-Coelho T A. Error analysis of a 3-DOF parallel mechanism for milling applications. *Journal of Mechanisms and Robotics*, 2013, 5(3): 034501

[9] Zhang Y, Ting K. Design and analysis of a spatial 3-DOF parallel manipulator with 2T1R-Type. *International Journal of Advanced Robotic Systems*, 2013, 10(3): 119-134

[10] Chen Q, Yu X, Li Q. Kinematics analysis of 2-PRU-PRRU parallel mechanism. In: Proceedings of the 2012 IEEE International Conference on Robotics and Biomimetics, Guangzhou, China, 2012. 2363-2368

[11] Xie F, Liu X J, Li T. A comparison study on the orientation capability and parasitic motions of two novel articulated tool heads with parallel kinematics. *Advances in Mechanical Engineering*, 2013, 4: 249103-249103

[12] Wu M, Zhang D, Zhao X. Kinematics analysis of a new parallel robot with asymmetrical architecture. *China Mechanical Engineering*, 2008, 19(12): 1423-1428 (In Chinese)

[13] Karouia M, Hervé J M. Asymmetrical 3-DOFspherical parallel mechanisms. *European Journal of Mechanics-A/Solids*, 2005, 24(1): 47-57

[14] Tsai M S, Yuan W H. Inverse dynamics analysis for a 3-PRS parallel mechanism based on a special decomposition of the reaction forces. *Mechanism and Machine Theory*, 2010, 45(11): 1491-1508

[15] Liu X J, Bonev I A. Orientation capability, error analysis, and dimensional optimization of two articulated tool heads with parallel kinematics. *Journal of Manufacturing Science and Engineering*, 2008, 130(1): 1-9

[16] Liu X J, Wang L P, Xie F, et al. Design of a three-axis articulated tool head with parallel kinematics achieving desired motion/force transmission characteristics. *Journal of Manufacturing Science and Engineering*, 2010, 132(2): 237-247

[17] Wang H, Fan K C. Identification of strut and assembly errors of a 3-PRS serial-parallel machine tool. *International Journal of Machine Tools and Manufacture*, 2004, 44(11): 1171-1178

[18] Hernandez A, Ibarreche J I, Petuya V, et al. Structural synthesis of 3-DOFspatial fully parallel manipulators. *International Journal of Advanced Robotic Systems*, 2014, 11(1). doi: 10.5772/58732

Liu Yuzhe, born in 1990. He has been a candidate of doctoral research since 2012 in Mechanical Engineering Department of Tsinghua University. He received his B. S. degree in Mechanical Science and Engineering School of Huazhong University of Science and Technology in 2012. His current research interests include parallel mechanisms and accuracy assurance.